RESEARCH ARTICLE | MAY 13 2025

Implementation of single-qubit gates with two rotations around axes in a plane

Yun-Pil Shim ; Edward Takyi; Jianjia Fei; Sangchul Oh ; Xuedong Hu ; Mark Friesen

APL Quantum 2, 026122 (2025)
https://doi.org/10.1063/5.0267247

APL Quantum ARTICLE pubs.aip.org/aip/apq

Implementation of single-qubit gates with two rotations around axes in a plane

Cite as: APL Quantum 2, 026122 (2025); doi: 10.1063/5.0267247
Submitted: 23 February 2025 • Accepted: 30 April 2025 •
Published Online: 13 May 2025

Yun-Pil Shim,[1,a)] Edward Takyi,[1] Jianjia Fei,[2] Sangchul Oh,[3] Xuedong Hu,[4] and Mark Friesen[2]

AFFILIATIONS

[1] Department of Physics, University of Texas at El Paso, El Paso, Texas 79968, USA
[2] Department of Physics, University of Wisconsin-Madison, Madison, Wisconsin 53706, USA
[3] Department of Physics, Southern Illinois University, Carbondale, Illinois 62901, USA
[4] Department of Physics, University at Buffalo, State University of New York, Buffalo, New York 14260, USA

[a)] **Author to whom correspondence should be addressed:** yshim@utep.edu

ABSTRACT

Typical experimental implementations of single-qubit gates involve two or three fixed rotation axes and up to three rotation steps. In this work, we prove that if the rotation axes can be tuned arbitrarily in a fixed plane, then two rotation steps are sufficient for implementing a single-qubit gate, and one rotation step is sufficient for implementing a state transformation. As concrete examples, we demonstrate two-step single-qubit gate implementations in two different physical qubit systems: (i) a transmon superconducting qubit coupled to an external microwave drive, such as a transmission line; and (ii) a quantum-dot based exchange-only qubit encoded in a three-spin block. These results provide a significant speedup for many common gate implementations, such as Rabi oscillations with phase control.

I. INTRODUCTION

In the quantum circuit model,[1] a universal quantum computer requires an entangling two-qubit gate, such as CNOT, and a set of single-qubit gates.[2] Although a finite set of quantum gates is sufficient for universality, fault-tolerant circuits require a large number of gates, even for very simple operations.[3] It is therefore important to be able to perform gate operations as efficiently as possible in order to minimize the effects of decoherence or gating errors.

Single-qubit operations can be viewed as rotations of the state vector of a qubit on a unit Bloch sphere.[3] The most efficient method for rotating a spin qubit would be to apply a magnetic field along the desired axis of rotation; however, this is not practical for most physical implementations. For example, to independently control an array of electron spin qubits in quantum dots with uniform g factors[4] would require an array of tunable micromagnets, which is experimentally challenging.

A more common approach is to provide two or three fixed, orthogonal rotation axes. This enables arbitrary rotations in up to three steps, e.g., by using an Euler-angle construction. Many qubit implementations employ this strategy. For single-spin qubits, this could involve a combination of Larmor rotations about the quantization ($\hat{z}$) axis and microwave-based Rabi oscillations around the $\hat{x}$ axis. For encoded qubits composed of two or more physical spins, it is possible for different physical coupling mechanisms to control different rotation axes on the Bloch sphere. For example, singlet–triplet logical qubits formed in double quantum dots use local magnetic field gradients to generate rotations about one axis and exchange interactions to generate rotations about an orthogonal axis.[5]

In this paper, we consider a common but slightly more general arrangement, where the rotation axes can point in any direction as long as they lie in a single plane. The quintessential gates of this type, which occur in many different qubit implementations, are Rabi oscillations with phase control, which provide arbitrary rotation axes in the x–y plane. As a concrete example of Rabi gates, we consider the widely studied superconducting transmon qubit,[6] for which single-qubit gate operations can be realized by coupling to an external microwave drive, such as a transmission line.[7–9]

As a second example, we consider exchange-only (EO) qubits encoded in a triple quantum dot.[10,11] Interesting features of these qubits include the fact that they are formed in decoherence-free subspaces and subsystems,[12–14] and they can be operated using only

fast exchange interactions.[15–17] There has been much experimental progress in EO qubits,[18–21] including improved experimental setups for a variety of different qubit implementations,[22–26] as well as demonstrations of logical gate operations.[27,28] Our derivations, below, build upon the known result that internal couplings between the physical spins in an EO qubit can be used to generate a continuous set of rotation axes in the x–z plane of the encoded qubit.[10] (A similar, single-plane rotation scheme is also possible for chirality-based logical qubits in a triple dot.[29]) We demonstrate that such single-plane rotations reduce the total number of steps required for single-qubit operations. For example, a state transformation, which maps a specific initial state onto a specific final state, can be accomplished in one step, while an arbitrary single-qubit rotation can be accomplished in two steps. We provide constructive proofs for both of these situations.

II. SINGLE-STEP STATE TRANSFORMATION

We first prove that a given initial state $|\Psi_A\rangle$ can be transformed to a specified state $|\Psi_B\rangle$, up to a physically insignificant global phase, by a single rotation about an axis in the x–z plane. The Bloch sphere geometry is shown in Fig. 1(a). Specifically, we want to determine the rotation axis $\hat{\mathbf{n}}$ and the rotation angle ϕ that satisfy

$$\mathscr{R}(\hat{\mathbf{n}},\phi)|\Psi_A\rangle = e^{i\eta}|\Psi_B\rangle, \tag{1}$$

where the rotation operator $\mathscr{R}(\hat{\mathbf{n}},\phi) = \exp(-i\boldsymbol{\sigma}\cdot\hat{\mathbf{n}}\phi/2)$ is defined in terms of the Pauli spin matrix vector $\boldsymbol{\sigma}$ and $e^{i\eta}$ is a global phase factor. The qubit state vectors $\hat{\mathbf{n}}_A$ and $\hat{\mathbf{n}}_B$ are also pictured on the Bloch sphere of Fig. 1(a). If the rotation axis is allowed to point in any direction (not just the x–z plane), then we could choose $\hat{\mathbf{n}} \propto (\hat{\mathbf{n}}_A + \hat{\mathbf{n}}_B)$ with $\phi = \pi$. We now show that the desired result can be achieved even when $\hat{\mathbf{n}}$ is confined to the x–z plane.

To perform a state transformation in a single step, it is clear that the rotation axis must be equidistant from both $\hat{\mathbf{n}}_A$ and $\hat{\mathbf{n}}_B$. This constraint defines a plane, given by $\hat{\mathbf{n}}\cdot(\hat{\mathbf{n}}_B - \hat{\mathbf{n}}_A) = 0$. On the other hand, we require the rotation axis to lie in the x–z plane, which is defined by $\hat{\mathbf{n}}\cdot\hat{\mathbf{y}} = 0$. The intersection of the two planes is given by

$$\hat{\mathbf{n}} = \frac{\hat{\mathbf{y}}\times(\hat{\mathbf{n}}_B - \hat{\mathbf{n}}_A)}{|\hat{\mathbf{y}}\times(\hat{\mathbf{n}}_B - \hat{\mathbf{n}}_A)|}. \tag{2}$$

Figure 1(b) shows the projection of $\hat{\mathbf{n}}_A$ and $\hat{\mathbf{n}}_B$ in the plane perpendicular to $\hat{\mathbf{n}}$. The inscribed angle is the angle of rotation, ϕ. Since the length of all three sides of the triangle are known, as indicated in the figure, we can obtain

$$\cos\phi = 1 - |\hat{\mathbf{n}}_B - \hat{\mathbf{n}}_A|^2/2L^2, \tag{3}$$

where $L = |\hat{\mathbf{n}}_A - (\hat{\mathbf{n}}\cdot\hat{\mathbf{n}}_A)\hat{\mathbf{n}}| = |\hat{\mathbf{n}}_B - (\hat{\mathbf{n}}\cdot\hat{\mathbf{n}}_B)\hat{\mathbf{n}}|$. The sign of ϕ is given by $\mathrm{sgn}[(\hat{\mathbf{n}}_A\times\hat{\mathbf{n}}_B)\cdot\hat{\mathbf{n}}]$. When the two planes are equivalent, we cannot use Eq. (2). However, in this special case, $\hat{\mathbf{n}}_A + \hat{\mathbf{n}}_B$ lies in the x–z plane, and we can simply choose $\hat{\mathbf{n}} \propto (\hat{\mathbf{n}}_A + \hat{\mathbf{n}}_B)$ with $\phi = \pi$.

Figure 1(a) shows an example of the state transformation procedure for the case $\hat{\mathbf{n}}_A = (0, \frac{\sqrt{2}}{2}, \frac{\sqrt{2}}{2})$ and $\hat{\mathbf{n}}_B = (\frac{\sqrt{2}}{2}, \frac{\sqrt{2}}{2}, 0)$. From Eqs. (2) and (3), we obtain the rotation axis $\hat{\mathbf{n}} = (\frac{\sqrt{2}}{2}, 0, \frac{\sqrt{2}}{2})$ and the rotation angle $\phi = -\cos^{-1}(1/3) \simeq -70.53°$.

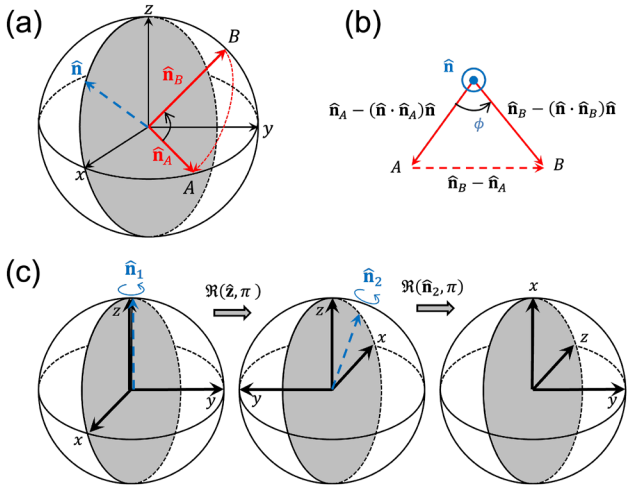

FIG. 1. Single-plane rotation method: the shaded regions indicate the x–z plane of the Bloch sphere, and dashed blue arrows indicate the rotation axes. (a) An arbitrary transformation, from the state $|\psi_A\rangle$ along $\hat{\mathbf{n}}_A$ to the state $|\psi_B\rangle$ along $\hat{\mathbf{n}}_B$, via a single rotation about the axis $\hat{\mathbf{n}}$. In this example, $\hat{\mathbf{n}}_A = (0,1,1)/\sqrt{2}$ and $\hat{\mathbf{n}}_B = (1,1,0)/\sqrt{2}$. (b) Projections of $\hat{\mathbf{n}}_A$ and $\hat{\mathbf{n}}_B$ in the plane perpendicular to $\hat{\mathbf{n}}$. As described in the main text, we obtain the rotation axis $\hat{\mathbf{n}} = (1,0,1)/\sqrt{2}$ and rotation angle $\phi = -\cos^{-1}(1/3)$. (c) An arbitrary single-qubit rotation, performed in two steps. In this example, $\mathscr{R}(\hat{\mathbf{y}},3\pi/2) = \mathscr{R}(\hat{\mathbf{n}}_2,\pi)\mathscr{R}(\hat{\mathbf{z}},\pi)$, with $\hat{\mathbf{n}}_2 = (-1,0,1)/\sqrt{2}$.

III. TWO-STEP QUBIT ROTATIONS

We now provide a constructive proof that any single-qubit gate (up to a global phase) can be generated in two rotation steps when the rotation axes point in an arbitrary direction in a single plane. Specifically, we want to solve for the rotation parameters defined by

$$\mathscr{R}(\hat{\mathbf{n}},\phi) = e^{i\eta}\mathscr{R}_2(\hat{\mathbf{n}}_2,\phi_2)\mathscr{R}_1(\hat{\mathbf{n}}_1,\phi_1), \tag{4}$$

where the rotation axis $\hat{\mathbf{n}}$ can point anywhere in the Bloch sphere, but the individual rotation axes $\hat{\mathbf{n}}_1$ and $\hat{\mathbf{n}}_2$ lie in the x–z plane. $e^{i\eta}$ is the global phase factor, which is physically insignificant but necessary for the mathematical formulation. It is convenient to work with angular coordinates defined by

$$\hat{\mathbf{n}} = (\sin\theta\cos\psi, \sin\theta\sin\psi, \cos\theta), \tag{5}$$

$$\hat{\mathbf{n}}_1 = (\sin\theta_1, 0, \cos\theta_1), \tag{6}$$

$$\hat{\mathbf{n}}_2 = (\sin\theta_2, 0, \cos\theta_2), \tag{7}$$

and illustrated in Fig. 2(a). Since an arbitrary rotation is characterized by three parameters (θ,ψ,ϕ), while the right-hand-side of Eq. (4) involves five parameters $(\eta,\theta_1,\phi_1,\theta_2,\phi_2)$, the equation is clearly under-constrained; many solutions exist, any of which suits our needs.

We now demonstrate that at least one solution exists by providing an explicit, analytical construction. We first simplify the problem by transforming to a new set of coordinate axes defined by the

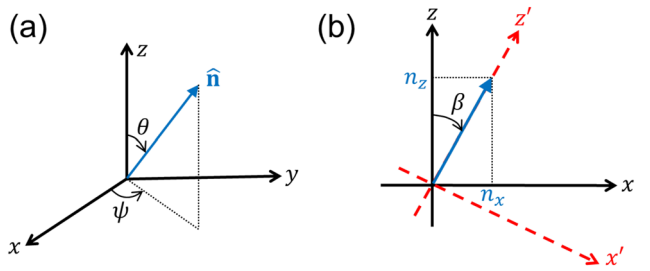

FIG. 2. Definition of the angular variables. (a) The logical rotation axis $\hat{\mathbf{n}}$, with the polar angle θ and the azimuthal angle ψ. (b) The projection of $\hat{\mathbf{n}}$ onto the x–z plane. We define a new coordinate system with axes x' and z' such that $n'_x = 0$ by rotating the x–z plane around the y axis by angle β.

projection of the logical rotation axis $\hat{\mathbf{n}}$ onto the x–z plane. The normalized projection becomes our new z axis unit vector $\hat{\mathbf{z}}'$, as shown in Fig. 2(b). The rotation angle for the transformation, β, is given by

$$\cos\beta = \frac{n_z}{\sqrt{n_x^2 + n_z^2}}, \quad \sin\beta = \frac{n_x}{\sqrt{n_x^2 + n_z^2}}, \tag{8}$$

where n_x and n_z are the components of $\hat{\mathbf{n}}$ in the original coordinate system. Using primed variables to indicate the new coordinate system, we have

$$\hat{\mathbf{n}} = \sin\theta'\hat{\mathbf{y}} + \cos\theta'\hat{\mathbf{z}}', \tag{9}$$

where θ' is given by

$$\sin\theta' = \sin\theta\,\sin\psi. \tag{10}$$

Note that $\hat{\mathbf{y}}$ is the same in both coordinate systems.

We now solve Eq. (4) in the primed coordinate system. Without loss of generality, we will restrict the two rotation axes to the range $\theta'_1, \theta'_2 \in [0, \pi)$ and the rotation angles to the range $\phi_1, \phi_2 \in [0, 2\pi)$ since a rotation with $\theta'_i \geq \pi$ by an angle ϕ_i is equivalent to the rotation with $\theta'_i - \pi$ by an angle $2\pi - \phi_i$. We can take advantage of the under-constrained nature of the problem by making the convenient choice $\phi_2 = \pi$. See Appendix B for detailed derivation. We then find

$$\theta'_2 = 0, \tag{11}$$

$$k\cos\theta'\sin\frac{\phi}{2} = \cos\frac{\phi_1}{2}, \tag{12}$$

$$k\sin\theta'\tan\frac{\phi}{2} = -\tan\theta'_1, \tag{13}$$

where $k = \mathrm{sgn}[n_y] = \mathrm{sgn}[\sin\theta\sin\psi]$. Here, θ'_2, ϕ_1, and θ'_1 are determined from Eqs. (11)–(13), respectively. These quantities are related to the original coordinate system through $\theta_1 = \theta'_1 + \beta$ and $\theta_2 = \theta'_2 + \beta$.

As noted above, Eqs. (11)–(13) do not represent unique solutions to Eq. (4). For example, we may obtain an alternative solution with the choice $\phi_1 = \pi$. After a similar analysis, we then obtain

$$\theta'_1 = 0, \tag{14}$$

$$-k\cos\theta'\sin\frac{\phi}{2} = \cos\frac{\phi_2}{2}, \tag{15}$$

$$k\sin\theta'\tan\frac{\phi}{2} = \tan\theta'_2. \tag{16}$$

To provide a practical comparison, we consider a conventional (Euler) method vs the single-plane method for the specific case of rotations around the y axis. For the Euler method, if we have two fixed axes of rotation ($\hat{\mathbf{x}}$ and $\hat{\mathbf{z}}$), the result corresponds to a three-step procedure given by $\mathscr{R}(\hat{\mathbf{y}}, \phi) = \mathscr{R}(\hat{\mathbf{z}}, \pi/2)\mathscr{R}(\hat{\mathbf{x}}, \phi)\mathscr{R}(\hat{\mathbf{z}}, -\pi/2)$. In contrast, the single-plane method is accomplished in just two steps, with $\mathscr{R}(\hat{\mathbf{y}}, \phi) = \mathscr{R}(\hat{\mathbf{n}}_2, \pi)\mathscr{R}(\hat{\mathbf{z}}, \pi)$, where $\hat{\mathbf{n}}_2 = (\sin\frac{\phi}{2}, 0, \cos\frac{\phi}{2})$. Figure 1(c) shows an explicit construction of a $3\pi/2$ rotation about the y axis, employing two rotations around axes in the x–z plane.

IV. ROTATIONS IN TRANSMON QUBITS

We now apply these results to a concrete physical example: the superconducting transmon qubit,[6] for which the single-qubit gate operations are implemented via a capacitive coupling to an external transmission line [see Fig. 3(a)]. In the frame that rotates at the qubit frequency, the driving Hamiltonian is given by[9]

$$\widehat{H}_d = -\frac{\Omega}{2}V_0(t)\begin{pmatrix} 0 & e^{-i(\delta\omega t-\phi)} \\ e^{i(\delta\omega t-\phi)} & 0 \end{pmatrix}, \tag{17}$$

where Ω is a constant defined by the device parameters, $V_0(t)$ is the envelope of the driving voltage $V(t) = V_0(t)\sin(\omega_d t + \phi)$, $\delta\omega = \omega_q - \omega_d$ is the detuning between the qubit frequency ω_q and the driving frequency ω_d, and ϕ is the phase of the driving voltage. If the drive is resonant with the qubit frequency (i.e., $\delta\omega = 0$), the Hamiltonian becomes

$$\widehat{H}_d = -\frac{\Omega}{2}V_0(t)[(\cos\phi)\sigma_x - (\sin\phi)\sigma_y], \tag{18}$$

corresponding to an arbitrary rotation axis in the x–y plane, defined by angle $-\phi$, measured from the positive x axis, and the qubit will oscillate between the two qubit states with a Rabi frequency of ΩV_0.

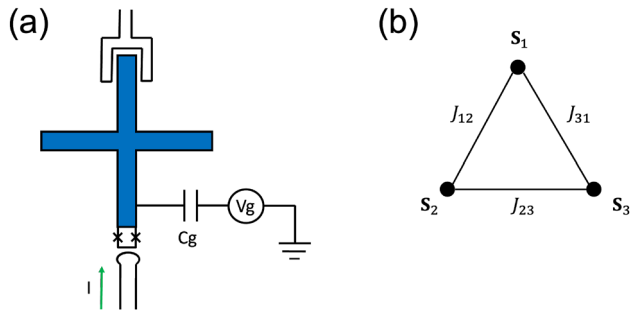

FIG. 3. Schematic descriptions of the two qubit implementations considered here. (a) An xmon-type transmon qubit. Here, the × shaped blue structure forms a superconducting capacitor connected on the bottom to a Josephson junction loop, coupled to an external current loop, and connected on the top to a resonator, allowing for single-qubit gate operations and readout. (b) An exchange-only qubit with three spins ($\mathbf{S}_1$–$\mathbf{S}_3$) coupled by pairwise exchange interactions (J_{12}, J_{23}, and J_{31}).

Here, we want to solve for the rotation parameters defined by

$$\mathscr{R}(\hat{\mathbf{n}},\phi) = e^{i\eta}\mathscr{R}_2(\hat{\mathbf{n}}_2,\phi_2)\mathscr{R}_1(\hat{\mathbf{n}}_1,\phi_1), \tag{19}$$

where $\hat{\mathbf{n}}$ is the desired rotation axis, which can point anywhere in the Bloch sphere, $e^{i\eta}$ is a global phase, and the physical rotation axes $\hat{\mathbf{n}}_1$ and $\hat{\mathbf{n}}_2$ lie in the x–y plane. The relevant axes are given by

$$\hat{\mathbf{n}} = (\sin\theta\cos\psi, \sin\theta\sin\psi, \cos\theta), \tag{20}$$

$$\hat{\mathbf{n}}_1 = (\cos\psi_1, \sin\psi_1, 0), \tag{21}$$

$$\hat{\mathbf{n}}_2 = (\cos\psi_2, \sin\psi_2, 0). \tag{22}$$

We now solve Eq. (19) for the five angular parameters $(\eta, \psi_1, \phi_1, \psi_2, \phi_2)$. We can obtain the situation described in Sec. III by rotating the x–y plane around the z axis by an angle ψ to obtain a new coordinate system, labeled x' and y'. In this primed coordinate system, we have $\psi \to \psi' = 0$ and $\psi_i \to \psi_i' = \psi_i - \psi$ for $i = 1, 2$. We then immediately obtain the desired results by setting $\phi_2 = 0$, obtaining the equations

$$\psi_2' = 0, \tag{23}$$

$$\sin\theta\sin\frac{\phi}{2} = k\cos\frac{\phi_1}{2}, \tag{24}$$

$$\cos\theta\tan\frac{\phi}{2} = -\tan\psi_1', \tag{25}$$

where $k = e^{i\eta} = \mathrm{sgn}[\cos(\phi_1/2)]$. Some specific examples of gates obtained from this two-step implementation are the Hadamard gate on the Bloch sphere, $H \equiv 1/\sqrt{2}[(1,1),(1,-1)]$, given by $H = i\mathscr{R}(\hat{\mathbf{x}},\pi)\mathscr{R}(\hat{\mathbf{y}},\pi/2)$, and a $\hat{\mathbf{z}}$-axis rotation, given by $\mathscr{R}(\hat{\mathbf{z}},\phi) = -\mathscr{R}(\hat{\mathbf{n}}_2,\pi)\mathscr{R}(\hat{\mathbf{x}},\pi)$, where $\hat{\mathbf{n}}_2 = (\cos(\phi/2), \sin(\phi/2), 0)$. In addition to the reduced number of rotational operations, the two-step implementation can also reduce the gate operation time. Since the direction of the rotation axis is purely determined by the phase of the driving field while the amplitude of the driving field is the same [see Eq. (18)], the gate operation time will be decided by the total rotation angles of the gate implementation. For example, the z-rotation above requires two π rotations (total rotation angle of 2π) in the two-step implementation, while the standard Euler angel composition would require three rotations, $\mathscr{R}(\hat{\mathbf{z}},\phi) = -\mathscr{R}(\hat{\mathbf{y}},3\pi/2)\mathscr{R}(\hat{\mathbf{x}},\phi)\mathscr{R}(\hat{\mathbf{y}},\pi/2)$, with a total rotation angle of $2\pi + \phi$.

V. ROTATIONS IN EXCHANGE-ONLY QUBITS

We also consider the example of an EO qubit encoded in a three-spin block [see Fig. 3(b)], for which all qubit operations are implemented using electrically tunable exchange couplings between the constituent spins, without requiring a magnetic field.[10]

We first show that the system Hamiltonian provides a continuous set of rotation axes in the x–z plane, which allows us to directly apply our main results. The effective Hamiltonian for the spin system is given by

$$\widehat{H} = J_{12}\mathbf{S}_1\cdot\mathbf{S}_2 + J_{23}\mathbf{S}_2\cdot\mathbf{S}_3 + J_{31}\mathbf{S}_3\cdot\mathbf{S}_1, \tag{26}$$

where the exchange coupling parameters J_{12}, J_{23}, and J_{31} are typically non-negative. The total spin S_{tot} and its z component S^z_{tot} are good quantum numbers since they commute with the Hamiltonian; we will use them to label the energy eigenstates. We are specifically interested in the states with $S_{\mathrm{tot}} = 1/2$ and $S^z_{\mathrm{tot}} = \pm 1/2$, which are two-fold degenerate. We specify these states as $\{|S_{\mathrm{tot}}, S^z_{\mathrm{tot}}; l\rangle\}$, adopting the label $l = 0,1$ for the degenerate states. With these definitions, we can encode the qubit in a decoherence-free subsystem as follows:[11]

$$|0\rangle_L = a\left|\frac{1}{2},\frac{1}{2};0\right\rangle + b\left|\frac{1}{2},-\frac{1}{2};0\right\rangle, \tag{27}$$

$$|1\rangle_L = a\left|\frac{1}{2},\frac{1}{2};1\right\rangle + b\left|\frac{1}{2},-\frac{1}{2};1\right\rangle, \tag{28}$$

where $|\frac{1}{2},\frac{1}{2};0\rangle = |S\rangle_{12}\otimes|\uparrow\rangle_3$, $|\frac{1}{2},\frac{1}{2};1\rangle = -\sqrt{1/3}|T_0\rangle_{12}\otimes|\uparrow\rangle_3 + \sqrt{2/3}|T_+\rangle_{12}\otimes|\downarrow\rangle_3$, and $|\frac{1}{2},-\frac{1}{2};0\rangle$ and $|\frac{1}{2},-\frac{1}{2};1\rangle$ are defined as the spin-flipped versions of $|\frac{1}{2},\frac{1}{2};0\rangle$ and $|\frac{1}{2},\frac{1}{2};1\rangle$, respectively.

In the encoded EO qubit space, the Hamiltonian becomes[30]

$$\widehat{H} = -\frac{J_{12}+J_{23}+J_{31}}{4}11 + \frac{\sqrt{3}(J_{23}-J_{31})}{4}\sigma_x + \frac{-2J_{12}+J_{23}+J_{31}}{4}\sigma_z. \tag{29}$$

The unitary operator $\widehat{U}(t) = \exp(-i\widehat{H}t/\hbar)$ rotates the EO qubit around an axis $\hat{\mathbf{n}}$ in the x–z plane by an angle ϕ, given by

$$\hat{\mathbf{n}} = \frac{1}{2J}\left(\sqrt{3}(J_{23}-J_{31}), 0, -2J_{12}+J_{23}+J_{31}\right), \tag{30}$$

$$\phi = Jt/\hbar, \tag{31}$$

where $J = \sqrt{J_{12}^2 + J_{23}^2 + J_{31}^2 - J_{12}J_{23} - J_{23}J_{31} - J_{31}J_{12}}$. Note that the rotation axis $\hat{\mathbf{n}}$ can be tuned in top-gated quantum dot devices by electrically controlling the exchange coupling constants J_{ij}; however, it always lies in the x-z plane. The decoherence-free subspace considered in Ref. 10 corresponds to the special case of $a = 1$ and $b = 0$ in Eqs. (27) and (28).

Equation (26) suggests a ring-like coupling configuration for the quantum dots [see Fig. 3(b)]. Such configurations have been achieved in the laboratory[31,32] with limited control of the couplings, and recent work[33] has demonstrated full control of the exchange interactions in a triangular triple quantum dot system. In these systems, we can directly apply the single-plane method described above.

A more common experimental arrangement is the linear triple quantum dot geometry, with one electron per dot. Recent work has demonstrated full control of all the exchange interactions in a six-dot device in a linear geometry.[34] In this linear geometry, however, since one of the exchange couplings in Eq. (26) is assumed to vanish, it is not possible to implement arbitrary rotations in the x–z plane; rather, only 2/3 of the plane is covered. For example, if $J_{31} = 0$ and $J_{12}, J_{23} \geq 0$, Eq. (30) indicates that rotations are limited to the range $\pi/3 \leq \theta \leq \pi$ and $0 \leq \theta \leq 2\pi/3$. Figure 4 shows the viable rotation axes in the x–z plane when one of the exchange couplings is set to zero.

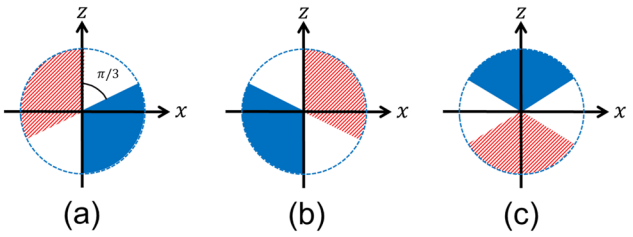

FIG. 4. Regions of the x–z plane where viable rotation axes are obtained when one of the three exchange couplings is set to zero: (a) $J_{31} = 0$, (b) $J_{23} = 0$, and (c) $J_{12} = 0$. Solid blue regions represent the rotation axes $\hat{\mathbf{n}}$, consistent with Eq. (30), assuming non-negative exchange couplings. Striped, red regions correspond to rotations around the $-\hat{\mathbf{n}}$ axis by angle ϕ, which is equivalent to rotations around $\hat{\mathbf{n}}$ by angle $2\pi - \phi$.

Despite the fact that we cannot perform rotations around axes over the entire x–z plane for the linear dot geometry, we note that many gates of interest can still be implemented in two or fewer steps. We demonstrate this by focusing on the configuration $J_{13} = 0$. In this case, rotations about the x axis $(J_{23} = 2J_{12})$ and the z axis $(J_{23} = 0)$ can be accomplished in a single step. Rotations around the y axis are nontrivial, however. Using the method described above, a $\hat{\mathbf{y}}$ rotation can be accomplished in two steps by using either one of the solutions,

$$\mathscr{R}(\hat{\mathbf{y}},\phi) = \mathscr{R}(\hat{\mathbf{z}},\pi)\mathscr{R}(\hat{\mathbf{n}}_1,\pi) = -\mathscr{R}(\hat{\mathbf{n}}_2,\pi)\mathscr{R}(\hat{\mathbf{z}},\pi), \qquad (32)$$

where $\hat{\mathbf{n}}_1 = (\sin\frac{\phi}{2}, 0, -\cos\frac{\phi}{2})$ and $\hat{\mathbf{n}}_2 = (\sin\frac{\phi}{2}, 0, \cos\frac{\phi}{2})$. Up to a global phase, the phase gate $S = [(1,0),(0,i)]$ and the $\pi/8$ gate $T = \{[(1,0),(0,\exp(i\pi/4)]\}$ can be implemented with single-step rotations around the z axis.

The Hadamard gate H corresponds to a rotation around an axis with $\theta = \pi/4$ and $\psi = 0$, by an angle $\phi = \pi$. For the configuration with $J_{12} = 0$, this can be implemented in a single step. However, in the $J_{23} = 0$ or $J_{31} = 0$ configurations, it cannot be implemented in fewer than three steps. If many Hadamard gates are required for a given quantum circuit, this could present a bottleneck. In this case, it might be preferable to change the encoded EO qubit basis in Eqs. (27) and (28) to one where qubits 2 and 3 are exchanged. In the latter configuration, the Hadamard gate is accomplished in one step.

We can compare our single-plane rotation method with the serial gating scheme for exchange-only qubits, which was described in Ref. 10. There, it was shown that when only one exchange coupling (J_{12}, J_{23}, or J_{31}) is allowed at a time, then a general logical qubit rotation requires three (four) steps for a ring (linear) geometry, as illustrated in Figs. 5(a) and 5(b). The single-plane rotation method described above can be viewed as a *parallel* gating scheme, where multiple exchange couplings are implemented simultaneously, as illustrated in Figs. 5(c) and 5(d). As we have shown, when two (three) exchange couplings are allowed simultaneously, then a logical qubit rotation requires three (two) steps. A comparison with Figs. 5(a) and 5(b) shows that the single-plane method is always more efficient than the serial gating scheme.

We can also compare the gate operation times of the parallel and serial implementations. As a concrete example, we consider the Hadamard gate for a ring geometry. In the parallel case [Fig. 5(c)], this can be implemented in a single step $H = i\mathscr{R}(\hat{\mathbf{n}},\pi)$ with

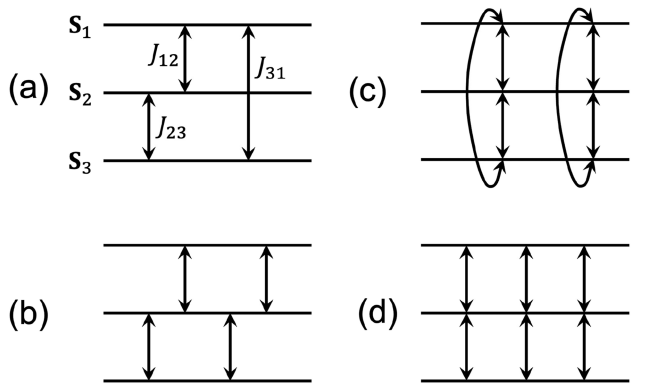

FIG. 5. Logical qubit rotation schemes for exchange-only logical qubits. The horizontal lines depict the three physical spins comprising the logical qubit, while the vertical arrows indicate exchange couplings between two spins. The gating scheme of Ref. 10 considers serial exchange couplings in (a) a ring geometry or (b) a linear geometry. The single-plane rotation scheme described here considers simultaneous, parallel exchange couplings in (c) a ring geometry or (d) a linear geometry. In the ring geometry, logical qubit gates require up to three steps in serial mode [(a)] and up to two steps in parallel mode [(c)]. In the linear geometry, logical qubit gates require up to four steps in the serial mode [(b)] and up to three steps in the parallel mode [(d)].

$\hat{\mathbf{n}} = \left(\frac{1}{\sqrt{2}}, 0, \frac{1}{\sqrt{2}}\right)$, which can be realized by taking $J_{12} = 0$ and $J_{31} = (2-\sqrt{3})J_{23}$. The total gate time would then be $t_H = \left(\frac{\sqrt{2}}{3-\sqrt{3}}\right)\left(\frac{\pi\hbar}{J_0}\right) \approx 1.12\left(\frac{\pi\hbar}{J_0}\right)$, where J_0 represents any of the J_{ij} when they are turned on. In the serial implementation of Fig. 5(a), it is not easy to obtain analytical solutions due to a large number of trigonometric functions to deal with, and we instead obtain numerical solutions using global optimization algorithms, yielding the best solution of $t_H \approx 3.02\left(\frac{\pi\hbar}{J_0}\right)$ and an average result of $t_H \approx 3.90\left(\frac{\pi\hbar}{J_0}\right)$. Thus, we conclude that the single-plane two-step gates can also lead to much faster gate operations.

VI. DISCUSSION

We have shown that the ability to tune qubit rotation axes in a single, fixed plane enables efficient, two-step implementations of single-qubit gates. This should be contrasted with fixed-axis methods (e.g., Euler-angles) that require up to three steps. Our results can be applied directly to any qubit schemes with flexible effective qubit rotation axis in a plane, such as transmon and EO qubits. Our scheme can also be adapted to any qubit implementation with at least partial control over the rotation axes. For example, the effective field corresponding to rotations of a singlet-triplet logical qubit[5] consists of a fixed B_x component and a tunable, positive B_z component. The resulting effective rotation axis covers about half of the x–z plane,[35,36] thus enabling efficient gating methods similar to those described here.

We note that a previous, unpublished version of some of our results was presented in Ref. 37. We further note that a recent manuscript has been posted, demonstrating a numerical approach that yields two-step single-qubit gate operations for EO qubits,

which supports our current findings.[38] That work also considers two-qubit gates, going beyond the results described here.

ACKNOWLEDGMENTS

This work was supported by the Defense Advanced Research Projects Agency (DARPA) QuEST program through Grant No. FA9550-09-1-0040 from the Air Force Office of Scientific Research (AFOSR), the Army Research Office (ARO) under Award Nos. W911NF0810482, W911NF1210607, W911NF0910393, W911NF2310018, W911NF2310110, and W911NF2420082, and the National Science Foundation (NSF) under Award No. 2316808. The views, conclusions, and recommendations contained in this document are those of the authors and are not necessarily endorsed nor should they be interpreted as representing the official policies, either expressed or implied, of the ARO or the U.S. Government. The U.S. Government is authorized to reproduce and distribute reprints for Government purposes notwithstanding any copyright notation herein.

AUTHOR DECLARATIONS

Conflict of Interest

The authors have no conflicts to disclose.

Author Contributions

Yun-Pil Shim: Conceptualization (equal); Formal analysis (lead); Funding acquisition (equal); Methodology (lead); Writing – original draft (equal). **Edward Takyi**: Formal analysis (supporting); Validation (equal); Writing – review & editing (equal). **Jianjia Fei**: Validation (equal); Writing – review & editing (equal). **Sangchul Oh**: Validation (equal); Writing – review & editing (equal). **Xuedong Hu**: Funding acquisition (equal); Validation (equal); Writing – review & editing (equal). **Mark Friesen**: Conceptualization (equal); Funding acquisition (equal); Validation (equal); Writing – original draft (equal).

DATA AVAILABILITY

Data sharing is not applicable to this article, as no new data were created or analyzed in this study.

APPENDIX A: ROTATION OPERATORS

A rotation operator $\mathscr{R}(\hat{\mathbf{n}}, \phi)$ is defined by its rotation axis $\hat{\mathbf{n}}$ and rotation angle ϕ. The rotation axis is described by a polar angle θ in the range $[0, \pi]$ and an azimuthal angle ψ in the range $[0, 2\pi]$, with

$$\hat{\mathbf{n}} = (\sin\theta\cos\psi, \sin\theta\sin\psi, \cos\theta). \tag{A1}$$

The rotation angle ϕ is also in the range $[0, 2\pi]$. In terms of Pauli operators, the rotation operator can be written as

$$\mathscr{R}(\hat{\mathbf{n}}, \phi) = \exp\left[-i\frac{\boldsymbol{\sigma}\cdot\hat{\mathbf{n}}}{2}\phi\right] = 11\cos\frac{\phi}{2} - i\boldsymbol{\sigma}\cdot\hat{\mathbf{n}}\sin\frac{\phi}{2}. \tag{A2}$$

Any rotation operator in a two-dimensional Hilbert space can be represented as

$$\mathscr{R} = a_0 11 + i(a_1\sigma_x + a_2\sigma_y + a_3\sigma_z), \tag{A3}$$

where $a_{0,1,2,3}$ are real constants. In matrix form,

$$\mathscr{R} = \begin{pmatrix} a_0 + ia_3 & a_2 + ia_1 \\ -a_2 + ia_1 & a_0 - ia_3 \end{pmatrix}. \tag{A4}$$

The unimodular condition requires that $a_0^2 + a_1^2 + a_2^2 + a_3^2 = 1$.

The necessary and sufficient condition for two rotation operators $\mathscr{R}_1 = a_0 11 + i(a_1\sigma_x + a_2\sigma_y + a_3\sigma_z)$ and $\mathscr{R}_2 = b_0 11 + i(b_1\sigma_x + b_2\sigma_y + b_3\sigma_z)$ to be identical is that $a_i = b_i$ for $i = 0, 1, 2, 3$. This is obvious by comparing the matrix elements of the two rotation operators.

APPENDIX B: TWO-STEP IMPLEMENTATIONS OF SINGLE-QUBIT GATES IN THE X–Z PLANE

We want to identify two sequential rotation steps around axes in the x–z plane that produce an arbitrary single-qubit gate up to a global phase,

$$\mathscr{R}(\hat{\mathbf{n}}, \phi) = e^{i\eta}\mathscr{R}(\hat{\mathbf{n}}_2, \phi_2)\mathscr{R}(\hat{\mathbf{n}}_1, \phi_1). \tag{B1}$$

According to the constraints discussed in the main text, $\hat{\mathbf{n}}$ can point any direction, while $\hat{\mathbf{n}}_1$ and $\hat{\mathbf{n}}_2$ must lie in the x–z plane,

$$\hat{\mathbf{n}} = (\sin\theta\cos\psi, \sin\theta\sin\psi, \cos\theta), \tag{B2}$$

$$\hat{\mathbf{n}}_1 = (\sin\theta_1, 0, \cos\theta_1), \tag{B3}$$

$$\hat{\mathbf{n}}_2 = (\sin\theta_2, 0, \cos\theta_2). \tag{B4}$$

We now transform the problem to a new set of (primed) coordinate axes, for which $\hat{\mathbf{n}}$ lies in the new y'–z' plane,

$$\hat{\mathbf{n}} = \sin\theta'\hat{\mathbf{y}}' + \cos\theta'\hat{\mathbf{z}}'. \tag{B5}$$

This can be achieved by rotating the original coordinate axes around the y axis (see Fig. 2 in the main text). Hence, the y axis is unaffected, while the $\hat{\mathbf{x}}$ and $\hat{\mathbf{z}}$ become $\hat{\mathbf{x}}'$ and $\hat{\mathbf{z}}'$, respectively. The rotation angle β for this transformation is given by

$$\cos\beta = \frac{n_z}{\sqrt{n_x^2 + n_z^2}}, \quad \sin\beta = \frac{n_x}{\sqrt{n_x^2 + n_z^2}}. \tag{B6}$$

In the primed coordinate system, we easily find that $\psi' = \pi/2$ when $n_y > 0$ and $\psi' = 3\pi/2$ when $n_y < 0$. θ' is obtained from

$$\sin\theta' = \sin\theta\sin\psi. \tag{B7}$$

Expanding both sides of Eq. (B1) in terms of Pauli operators and matching their coefficients, we obtain the following relations in the primed coordinate system:

$$\cos\frac{\phi}{2} = e^{i\eta}\left[\cos\frac{\phi_2}{2}\cos\frac{\phi_1}{2} - \cos(\theta_2' - \theta_1')\sin\frac{\phi_2}{2}\sin\frac{\phi_1}{2}\right], \quad \text{(B8)}$$

$$0 = e^{i\eta}\left[\sin\theta_1'\cos\frac{\phi_2}{2}\sin\frac{\phi_1}{2} + \sin\theta_2'\sin\frac{\phi_2}{2}\cos\frac{\phi_1}{2}\right], \quad \text{(B9)}$$

$$k\sin\theta'\sin\frac{\phi}{2} = e^{i\eta}\left[-\sin(\theta_2' - \theta_1')\sin\frac{\phi_2}{2}\sin\frac{\phi_1}{2}\right], \quad \text{(B10)}$$

$$\cos\theta'\sin\frac{\phi}{2} = e^{i\eta}\left[\cos\theta_1'\cos\frac{\phi_2}{2}\sin\frac{\phi_1}{2} + \cos\theta_2'\sin\frac{\phi_2}{2}\cos\frac{\phi_1}{2}\right]. \quad \text{(B11)}$$

Here, we define $k = \mathrm{sgn}[n_y] = \mathrm{sgn}[\sin\theta\sin\psi]$. Numerical results suggest that there will be a continuum of solutions for these equations. Here, we set $\phi_2 = \pi$ to simplify the equations and to enable an analytical solution. In this case, the equations reduce to

$$\cos\frac{\phi}{2} = -e^{i\eta}\cos(\theta_2' - \theta_1')\sin\frac{\phi_1}{2}, \quad \text{(B12)}$$

$$0 = e^{i\eta}\sin\theta_2'\cos\frac{\phi_1}{2}, \quad \text{(B13)}$$

$$k\sin\theta'\sin\frac{\phi}{2} = -e^{i\eta}\sin(\theta_2' - \theta_1')\sin\frac{\phi_1}{2}, \quad \text{(B14)}$$

$$\cos\theta'\sin\frac{\phi}{2} = e^{i\eta}\cos\theta_2'\cos\frac{\phi_1}{2}. \quad \text{(B15)}$$

From Eq. (B13), we see that either $\sin\theta_2' = 0$ or $\cos\frac{\phi_1}{2} = 0$. To satisfy Eq. (B15), we must have $\sin\theta_2' = 0$. We, therefore, obtain $\theta_2' = 0$.

The three remaining equations are

$$\cos\frac{\phi}{2} = -e^{i\eta}\cos\theta_1'\sin\frac{\phi_1}{2}, \quad \text{(B16)}$$

$$k\sin\theta'\sin\frac{\phi}{2} = e^{i\eta}\sin\theta_1'\sin\frac{\phi_1}{2}, \quad \text{(B17)}$$

$$\cos\theta'\sin\frac{\phi}{2} = e^{i\eta}\cos\frac{\phi_1}{2}. \quad \text{(B18)}$$

From Eq. (B17), we see that $e^{i\eta} = k$ since the sine functions are all positive for the range of angles $\theta', \theta_1' \in [0, \pi]$ and $\phi, \phi_1 \in [0, 2\pi]$. Hence,

$$k\cos\frac{\phi}{2} = -\cos\theta_1'\sin\frac{\phi_1}{2}, \quad \text{(B19)}$$

$$\sin\theta'\sin\frac{\phi}{2} = \sin\theta_1'\sin\frac{\phi_1}{2}, \quad \text{(B20)}$$

$$k\cos\theta'\sin\frac{\phi}{2} = \cos\frac{\phi_1}{2}. \quad \text{(B21)}$$

Here, we have two unknowns (θ_1' and ϕ_1) and three equations. However, the three equations are not independent. By squaring both sides of Eqs. (B19) and (B20) and adding them, we obtain

$$\cos^2\frac{\phi}{2} + \sin^2\theta'\sin^2\frac{\phi}{2} = \sin^2\frac{\phi_1}{2}, \quad \text{(B22)}$$

which leads to

$$\cos^2\theta'\sin^2\frac{\phi}{2} = \cos^2\frac{\phi_1}{2}. \quad \text{(B23)}$$

This is the same as the square of Eq. (B21). We can obtain another equation by dividing Eq. (B20) by Eq. (B19),

$$k\sin\theta'\tan\frac{\phi}{2} = -\tan\theta_1'. \quad \text{(B24)}$$

We now show that once θ_1' and ϕ_1 are obtained, by solving Eqs. (B21) and (B24), the results will also satisfy Eqs. (B19) and (B20). If we represent the left-hand side (right-hand side) of Eq. (B19) as L_1 (R_1) and similarly for L_2 (R_2) in Eq. (B20), then Eq. (B21) implies that $L_1^2 + L_2^2 = R_1^2 + R_2^2$, and Eq. (B24) leads to $L_2/L_1 = R_2/R_1 \equiv \gamma$. Here, we note that L_2 and R_2 are both positive, as was explained below Eq. (B17). Plugging $L_1 = L_2/\gamma$ and $R_1 = R_2/\gamma$ into $L_1^2 + L_2^2 = R_1^2 + R_2^2$, we obtain $(1/\gamma^2 + 1)L_2^2 = (1/\gamma^2 + 1)R_2^2$, and then, $L_2^2 = R_2^2$. Since L_2 and R_2 are positive, we obtain $L_2 = R_2$. Now, from $L_2/L_1 = R_2/R_1$, we obtain $L_1 = R_1$. We can therefore determine ϕ_1 from Eq. (B21) and θ_1' from Eq. (B24). Note that Eqs. (B21) and (B24) uniquely determine ϕ_1 in the range $[0, 2\pi]$ and θ_1' in the range $[0, \pi]$.

To summarize, we can always implement an arbitrary single-qubit gate with two rotation steps around axes in the x–z plane, given by $\phi_2 = \pi$ and $\theta_2' = 0$, with ϕ_1 obtained from Eq. (B21) and θ_1' obtained from Eq. (B24). Of course, this is not the only solution. For example, we can also find a solution by choosing $\phi_1 = \pi$. In that case, $\theta_1' = 0$, $e^{i\eta} = -k$, and after a similar procedure, we obtain

$$-k\cos\theta'\sin\frac{\phi}{2} = \cos\frac{\phi_2}{2}, \quad \text{(B25)}$$

$$k\sin\theta'\tan\frac{\phi}{2} = \tan\theta_2', \quad \text{(B26)}$$

which determine θ_2' and ϕ_2 uniquely. Once we determine θ_1' and θ_2', we can transform back to the original coordinate system using $\theta_1 = \theta_1' + \beta$ and $\theta_2 = \theta_2' + \beta$.

REFERENCES

[1] D. Deutsch, "Quantum computational networks," Proc. R. Soc. London A **425**, 73 (1989).

[2] D. P. DiVincenzo, "Two-bit gates are universal for quantum computation," Phys. Rev. A **51**, 1015–1022 (1995).

[3] M. A. Nielsen and I. L. Chuang, *Quantum Computation and Quantum Information* (Cambridge University Press, 2000).

[4] D. Loss and D. P. DiVincenzo, "Quantum computation with quantum dots," Phys. Rev. A **57**, 120 (1998).

[5] J. R. Petta, A. C. Johnson, J. M. Taylor, E. A. Laird, A. Yacoby, M. D. Lukin, C. M. Marcus, M. P. Hanson, and A. C. Gossard, "Coherent manipulation of coupled electron spins in semiconductor quantum dots," Science **309**, 2180–2184 (2005).

[6] J. Koch, T. M. Yu, J. Gambetta, A. A. Houck, D. I. Schuster, J. Majer, A. Blais, M. H. Devoret, S. M. Girvin, and R. J. Schoelkopf, "Charge-insensitive qubit design derived from the cooper pair box," Phys. Rev. A **76**, 042319 (2007).

[7] P. Krantz, M. Kjaergaard, F. Yan, T. P. Orlando, S. Gustavsson, and W. D. Oliver, "A quantum engineer's guide to superconducting qubits," Appl. Phys. Rev. **6**, 021318 (2019).

[8]M. Kjaergaard, M. E. Schwartz, J. Braumüller, P. Krantz, J. I.-J. Wang, S. Gustavsson, and W. D. Oliver, "Superconducting qubits: Current state of play," Annu. Rev. Condens. Matter Phys. **11**, 369–395 (2020).
[9]S. E. Rasmussen, K. S. Christensen, S. P. Pedersen, L. B. Kristensen, T. Bækkegaard, N. J. S. Loft, and N. T. Zinner, "Superconducting circuit companion—an introduction with worked examples," PRX Quantum **2**, 040204 (2021).
[10]D. P. DiVincenzo, D. Bacon, J. Kempe, G. Burkard, and K. B. Whaley, "Universal quantum computation with the exchange interaction," Nature **408**, 339 (2000).
[11]B. H. Fong and S. M. Wandzura, "Universal quantum computation and leakage reduction in the 3-Qubit decoherence free subsystem," Quantum Inf. Comput. **11**, 1003 (2011).
[12]P. Zanardi and M. Rasetti, "Noiseless quantum codes," Phys. Rev. Lett. **79**, 3306–3309 (1997).
[13]L.-M. Duan and G.-C. Guo, "Reducing decoherence in quantum-computer memory with all quantum bits coupling to the same environment," Phys. Rev. A **57**, 737–741 (1998).
[14]D. A. Lidar, I. L. Chuang, and K. B. Whaley, "Decoherence-free subspaces for quantum computation," Phys. Rev. Lett. **81**, 2594–2597 (1998).
[15]D. Bacon, J. Kempe, D. A. Lidar, and K. B. Whaley, "Universal fault-tolerant quantum computation on decoherence-free subspaces," Phys. Rev. Lett. **85**, 1758–1761 (2000).
[16]J. Kempe, D. Bacon, D. A. Lidar, and K. B. Whaley, "Theory of decoherence-free fault-tolerant universal quantum computation," Phys. Rev. A **63**, 042307 (2001).
[17]J. Kempe, D. Bacon, D. P. DiVincenzo, and K. B. Whaley, "Encoded universality from a single physical interaction," Quantum Inf. Comput. **1**, 33–55 (2001).
[18]J. M. Taylor, V. Srinivasa, and J. Medford, "Electrically protected resonant exchange qubits in triple quantum dots," Phys. Rev. Lett. **111**, 050502 (2013).
[19]J. Medford, J. Beil, J. M. Taylor, E. I. Rashba, H. Lu, A. C. Gossard, and C. M. Marcus, "Quantum-dot-based resonant exchange qubit," Phys. Rev. Lett. **111**, 050501 (2013).
[20]A. C. Doherty and M. P. Wardrop, "Two-qubit gates for resonant exchange qubits," Phys. Rev. Lett. **111**, 050503 (2013).
[21]Y.-P. Shim and C. Tahan, "Charge-noise-insensitive gate operations for always-on, exchange-only qubits," Phys. Rev. B **93**, 121410(R) (2016).
[22]J. Medford, J. Beil, J. M. Taylor, S. D. Bartlett, A. C. Doherty, E. I. Rashba, D. P. DiVincenzo, H. Lu, A. C. Gossard, and C. M. Marcus, "Self-consistent measurement and state tomography of an exchange-only spin qubit," Nat. Nanotechnol. **8**, 654–659 (2013).
[23]K. Eng, T. D. Ladd, A. Smith, M. G. Borselli, A. A. Kiselev, B. H. Fong, K. S. Holabird, T. M. Hazard, B. Huang, P. W. Deelman, I. Milosavljevic, A. E. Schmitz, R. S. Ross, M. F. Gyure, and A. T. Hunter, "Isotopically enhanced triple-quantum-dot qubit," Sci. Adv. **1**, e1500214 (2015).
[24]E. A. Laird, J. M. Taylor, D. P. DiVincenzo, C. M. Marcus, M. P. Hanson, and A. C. Gossard, "Coherent spin manipulation in an exchange-only qubit," Phys. Rev. B **82**, 075403 (2010).
[25]W. Ha, S. D. Ha, M. D. Choi, Y. Tang, A. E. Schmitz, M. P. Levendorf, K. Lee, J. M. Chappell, T. S. Adams, D. R. Hulbert, E. Acuna, R. S. Noah, J. W. Matten, M. P. Jura, J. A. Wright, M. T. Rakher, and M. G. Borselli, "A flexible design platform for Si/SiGe exchange-only qubits with low disorder," Nano Lett. **22**, 1443–1448 (2022).
[26]J. Z. Blumoff, A. S. Pan, T. E. Keating, R. W. Andrews, D. W. Barnes, T. L. Brecht, E. T. Croke, L. E. Euliss, J. A. Fast, C. A. C. Jackson, A. M. Jones, J. Kerckhoff, R. K. Lanza, K. Raach, B. J. Thomas, R. Velunta, A. J. Weinstein, T. D. Ladd, K. Eng, M. G. Borselli, A. T. Hunter, and M. T. Rakher, "Fast and high-fidelity state preparation and measurement in triple-quantum-dot spin qubits," PRX Quantum **3**, 010352 (2022).
[27]R. W. Andrews, C. Jones, M. D. Reed, A. M. Jones, S. D. Ha, M. P. Jura, J. Kerckhoff, M. Levendorf, S. Meenehan, S. T. Merkel, A. Smith, B. Sun, A. J. Weinstein, M. T. Rakher, T. D. Ladd, and M. G. Borselli, "Quantifying error and leakage in an encoded Si/SiGe triple-dot qubit," Nat. Nanotechnol. **14**, 747–750 (2019).
[28]A. J. Weinstein, M. D. Reed, A. M. Jones, R. W. Andrews, D. Barnes, J. Z. Blumoff, L. E. Euliss, K. Eng, B. H. Fong, S. D. Ha, D. R. Hulbert, C. A. C. Jackson, M. Jura, T. E. Keating, J. Kerckhoff, A. A. Kiselev, J. Matten, G. Sabbir, A. Smith, J. Wright, M. T. Rakher, T. D. Ladd, and M. G. Borselli, "Universal logic with encoded spin qubits in silicon," Nature **615**, 817–822 (2023).
[29]C.-Y. Hsieh and P. Hawrylak, "Quantum circuits based on coded qubits encoded in chirality of electron spin complexes in triple quantum dots," Phys. Rev. B **82**, 205311 (2010).
[30]Y. S. Weinstein and C. S. Hellberg, "Energetic suppression of decoherence in exchange-only quantum computation," Phys. Rev. A **72**, 022319 (2005).
[31]L. Gaudreau, S. A. Studenikin, A. S. Sachrajda, P. Zawadzki, A. Kam, J. Lapointe, M. Korkusinski, and P. Hawrylak, "Stability diagram of a few-electron triple dot," Phys. Rev. Lett. **97**, 036807 (2006).
[32]S. Amaha, T. Hatano, T. Kubo, S. Teraoka, Y. Tokura, S. Tarucha, and D. G. Austing, "Stability diagrams of laterally coupled triple vertical quantum dots in triangular arrangement," Appl. Phys. Lett. **94**, 092103 (2009).
[33]E. Acuna, J. D. Broz, K. Shyamsundar, A. B. Mei, C. P. Feeney, V. Smetanka, T. Davis, K. Lee, M. D. Choi, B. Boyd, J. Suh, W. Ha, C. Jennings, A. S. Pan, D. S. Sanchez, M. D. Reed, and J. R. Petta, "Coherent control of a triangular exchange-only spin qubit," Phys. Rev. Applied **22** (2024).
[34]S. G. J. Philips, M. T. Mądzik, S. V. Amitonov, S. L. de Snoo, M. Russ, N. Kalhor, C. Volk, W. I. L. Lawrie, D. Brousse, L. Tryputen, B. P. Wuetz, A. Sammak, M. Veldhorst, G. Scappucci, and L. M. K. Vandersypen, "Universal control of a six-qubit quantum processor in silicon," Nature **609**, 919–924 (2022).
[35]X. Wang, L. S. Bishop, J. P. Kestner, E. Barnes, K. Sun, and S. Das Sarma, "Composite pulses for robust universal control of singlet–triplet qubits," Nat. Commun. **3**, 997 (2012).
[36]J. P. Kestner, X. Wang, L. S. Bishop, E. Barnes, and S. Das Sarma, "Noise-resistant control for a spin qubit array," Phys. Rev. Lett. **110**, 140502 (2013).
[37]Y.-P. Shim, J. Fei, S. Oh, X. Hu, and M. Friesen, "Single-qubit gates in two steps with rotation axes in a single plane," arXiv:1303.0297 [cond-mat.mes-hall] (2013).
[38]I. Heinz, F. Borjans, M. Curry, R. Kotlyar, F. Luthi, M. T. Mądzik, F. A. Mohiyaddin, N. Bishop, and G. Burkard, "Fast quantum gates for exchange-only qubits using simultaneous exchange pulses," arXiv:2409.05843 [quant-ph] (2024).